Manipulating the shape of flexible magnetic nanodisks with meronlike magnetic states

Beatriz Miranda-Silva [1], Pedro H. C. Taveira [1], Allison W. Teixeira [1], Jakson M. Fonseca [1], Leonarde N. Rodrigues,[1]
Ricardo G. Elías [2,3], Alejandro Riveros [4], Nicolás Vidal-Silva [5], and Vagson L. Carvalho-Santos [1]

[1]*Departamento de Física, Universidade Federal de Viçosa, Avenida Peter Henry Rolfs s/n, 36570-000, Viçosa, Minas Gerais, Brazil*
[2]*Departamento de Física, Universidad de Santiago de Chile (USACH), Avenida Ecuador 3493, Estación Central, Santiago, Chile*
[3]*Center for the Development of Nanoscience and Nanotechnology, Avenida Libertador Bernardo O'Higgins 3363, 9170124 Santiago, Chile*
[4]*Escuela de Ingeniera, Universidad Central de Chile, 8330601 Santiago, Chile*
[5]*Departamento de Ciencias Físicas, Universidad de La Frontera, Casilla 54-D, 4811186 Temuco, Chile*

The control of the magnetic properties of shapeable devices and the manipulation of flexible structures by external magnetic fields is a keystone of future magnetoelectronics-based devices. In this work we study the elastic properties of a flexible magnetic nanodisk that hosts a meron as the magnetic state and can be deformed from structures with positive to negative Gaussian curvature. We show that the winding number of the hosted meron is crucial to determine the curvature sign of the stable obtained shape. Additionally, we show that the curvature that minimizes the total energy of the nanodisk depends on geometrical and mechanical parameters. It is shown that an increase in the external radius and Young's modulus leads to a decrease in the curvature absolute value. Finally, it is shown that the nanodisk's shape also depends on the connection between the polarity and chirality of the meronlike state.

I. INTRODUCTION

The possibility to reshape electronic systems has promoted the concept of flexible and stretchable electronics to a hot topic in soft matter research [1,2]. This class of structures has been explored as applications of shapeable systems in sensory devices [3–6], solar cells [7], electronic skins [3,8–10], soft robotics [11], wearable devices [12], and for manipulating the shape of liquid interfaces [13]. Also, the inclusion of the magnetic degree of freedom into soft systems is fascinating because there are several possibilities to manipulate the magnetic properties by changing the system's shape or to produce effects on the geometry of the system by applying external magnetic stimuli [1]. For instance, one can cite the possibility of using stretchable magnetoelectronics for the emerging field of soft robotics [11], and manipulating the shape of elastomeric actuators [14,15].

In general, most field-controllable materials with magnetically switchable properties consist of elastomers, which are magnetic nanoparticles embedded into a nonmagnetizable polymer matrix [16]. Because the intrinsic properties of the magnetic particles do not affect the other ones, the proper description of the magnetic properties of elastomers is performed by considering a dipole-dipole interaction [17]. Therefore, when an external magnetic field is applied to the system, there are particle rearrangements, which changes the mechanical properties of the elastomer matrix [18]. As a result, both the external field and initial arrangement of the magnetic particles influence the final stabilized shape of the magnetic elastomer [19]. In this case, the competition between magnetic interactions with membrane bending and stretching can drive the membrane to expand, contract, or twist in such a way that many shapes can be obtained as a function of an external magnetic field [15,20].

Nevertheless, the imbibition of magnetic microparticles in an elastic matrix avoids the possibility of leading with flexible magnetic systems in the nanoscale range of sizes. This problem can be circumvented by constructing systems where a short-range exchange plays the role. Examples of such systems include organic, organic-inorganic hybrid, and molecule-based magnets, which exhibit different types of magnetic ordering [21–24], even in a room-temperature environment [25]. Therefore, due to the short range of magnetic interactions, one can reduce the size of the flexible magnetic system whose shape can be manipulated by external magnetic fields. Theoretical works have considered magnetic subsystems where the short-range exchange interaction determines the magnetic properties of the particle, and stretching and bending are responsible for describing the energetic cost to deform the elastic subsystem. In this case, the nucleation of periodic solitons in the magnetic system induces the appearance of periodic shrinking of the membrane [26], and curvature-induced geometrical frustration in magnetic systems in both cases under the absence and presence of external magnetic fields [27–30]. By considering flexible systems whose properties are controlled by short-range interactions, Yershov *et al.* [31] showed that a unidimensional flexible magnetic ring presents a shape depending on the magnetic configuration. An onion or a vortex magnetic state leads the nanoring to assume an elliptical or circular shape, respectively. Additionally, due to the magnetochirality induced by the intrinsic Dzyaloshinskii-Moriya interaction (DMI), a flexible ribbon can be spontaneously deformed [32]. This ribbon deformation depends on the symmetry of the DMI and the

mechanical, magnetic, and geometric parameters of the flexible magnetic body.

Regarding magnetic properties, it is known that the introduction of curvature in quasi-2D systems induces effective interactions [33] that are responsible, for instance, for a curvature-driven polarity-chirality connection for vortex [34] and skyrmion [35,36]. These effective interactions also yield a curvature-induced selection on the domain wall phase [37–39], and the nucleation of a vortex/antivortex pair in toroidal nanoshells [40]. The exchange-driven curvature induced polarity-chirality connection was evidenced by Elías *et al.* [41], who have shown the existence of a curvature-induced winding number of merons hosted in rigid curved magnetic elements, where vortices and antivortices are nucleated in structures with positive and negative Gaussian curvatures, respectively. The authors also showed that the minimum energy configuration of the meron depends on the relative directions defined by the meron's polarity and chirality. Nevertheless, in that work, the range of considered parameters leads to minimum magnetic energy for the maximum (vortex) and minimum (antivortex) curvatures. Based on these results, if we consider that the considered structures are flexible, the new freedom degree brought by the elastic subsystem should yield an optimum value for the curvature minimizing the energy. Therefore, in this work, we propose the study of the static magnetic and mechanical properties of a flexible magnetic disk hosting a meron as the magnetic state. It is shown that the modulus of the optimum curvature of the stable structure decreases as the disk radius increases. As expected, the mechanical properties of the elastic subsystem also influence the obtained stable shape. Indeed, due to the increase in the structure rigidity, the optimum curvature decreases as Young's modulus increases. We also show that the proper control of the meron's chirality can be used to deform the shape of the disk from a paraboloidal structure, with positive curvature, to a saddle-like shape, with negative Gaussian curvature.

This work is divided as follows: Section II presents the adopted theoretical model to describe the flexible magnetic disk. In Sec. III we present the obtained results and discussions. Section IV brings our conclusions and prospects.

II. THEORETICAL MODEL

In this work we analyze a flexible magnetic nanodisk, defined as a nanostructure with magnetic and elastic degrees of freedom interacting and exhibiting a meron as a metastable magnetic configuration. Although the stray field energy of the infinite thin film provides an effective easy-plane anisotropy, resulting in the single-domain ground state [42], planar vortices can appear as topological states in planar and curved spin systems described by the anisotropic Heisenberg model (*XY* model) [30,43–45]. Nevertheless, because magnetic vortices described by the anisotropic Heisenberg model develop an out-of-plane component to the magnetization, avoiding spurious divergences from the exchange interaction, the meronlike magnetic configurations described in our theoretical model do not have topological stability, appearing as metastable states of quasi-2D systems. One of the main features of a metastable state relies on the fact that it has a
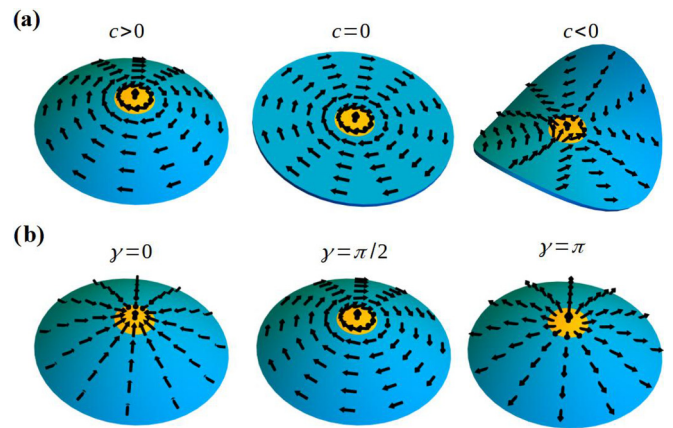

FIG. 1. Schematic representation of the considered geometry with $R = 10\ell$ and $h = 0.1\ell$. In (a), from left to right, we present the geometries for $c = 2 \times 10^3$ m$^{-1/2}$, 0, and -2×10^3 m$^{-1/2}$. The vector field of the parabola and disk consists of a meron with $q = 1$ and $\gamma = \pi/2$, while the magnetization field in the surface negative curvature is a meron with $q = -1$ and $\gamma = \pi/2$. Panel (b) depicts a meron with $q = 1$ and different values of γ hosted in the paraboloidal surface. Yellow region depicts a circumference of radius r_0, representing the meron's core.

finite lifetime, after which the system goes toward a state with lower energy. Therefore, merons can be, at least, artificially imposed and hosted in a nanodisk. For instance, these magnetization patterns have been explicitly named as metastable states in previous works [46,47]. Following these ideas, the stability of the meronlike configurations is not considered in this work, and some of the analyzed magnetic states could not be naturally observed. Thus, we assume distinct magnetic configurations as metastable states without paying special attention to how such metastability was reached. We assume that the nanostructure consists of a thin shell, whose thickness h is much smaller than the external radius R of the disk ($h \ll R$). In this context, the border effects can be neglected, and the magnetostatic energy can be safely approximated by an effective in-surface anisotropy [42].

The geometrical description of the considered system is given by

$$\mathbf{r} = x\hat{\mathbf{x}} + y\hat{\mathbf{y}} + c(cx^2 + |c|y^2)\hat{\mathbf{z}}, \quad (1)$$

where $x = \rho \cos\phi$, $y = \rho \sin\phi$, $\rho \in [0, R]$, $\phi \in [0, 2\pi]$, $\{\mathbf{x}, \mathbf{y}, \mathbf{z}\}$ corresponds to the unitary vectors of the three-dimensional Cartesian space, and $c \in [-\infty, \infty]$ is a number that determines the surface curvature, given by

$$\mathcal{K} = \frac{4c^3|c|}{[1 + 4c^4(x^2 + y^2)]^2}. \quad (2)$$

Therefore, $c < 0$ describes a hyperbolic paraboloid, which has a negative Gaussian curvature, and $c > 0$ defines a paraboloidal surface, presenting a positive Gaussian curvature. If $c = 0$, the parametrization describes a planar nanodisk. Figure 1(a) depicts the shapes of the flexible magnetic structures for the cases $c = 2 \times 10^3$ m$^{-1/2}$, $c = 0$, and $c = -2 \times 10^3$ m$^{-1/2}$, evidencing the relation between the sign of c and the surface shape.

To properly describe the magnetic properties of the nanodisk, we use the micromagnetic approach, in which the magnetization is a continuous function of the position inside the magnetic element. Therefore, the magnetization field can be parametrized as a spherical coordinate system lying in a curvilinear basis, that is,

$$\mathbf{M} = \cos\Phi \sin\Theta \vec{\rho} + \sin\Phi \sin\Theta \vec{\phi} + \cos\Theta \vec{n}, \qquad (3)$$

where $\vec{\rho} = \mathbf{g}_\rho / \|\mathbf{g}_\rho\|$ and $\vec{\phi} = \mathbf{g}_\phi / \|\mathbf{g}_\phi\|$ are unitary vectors pointing along the tangential direction on the surface, and $\vec{n} = \vec{\rho} \times \vec{\phi}$ is the unitary vector pointing perpendicularly to the surface. Because the parametrization given in Eq. (1) yields a nonorthogonal basis, the radial direction in the surface $\vec{\rho}$ is not necessarily orthogonal to $\vec{\phi}$. Here, we define the natural tangential basis $\mathbf{g}_\mu = \partial_\mu \mathbf{r}$ with $\partial_\mu \equiv \frac{\partial}{\partial x_i}$, $i = 1, 2$, from which one can obtain the metric tensor elements $g_{\mu\nu} = \mathbf{g}_\mu \cdot \mathbf{g}_\nu$.

In the considered parametrization, $\mathbf{M}$ has not, in general, a constant modulus. Thus, it is convenient to define the normalized magnetization, given by $\mathbf{m} = \mathbf{M}/\|\mathbf{M}\|$, with $\|\mathbf{M}\| = \sqrt{1 + \sin(2\Phi)(\cos^2\Theta)\vec{\rho} \cdot \vec{\phi}}$. Following the ideas presented in Ref. [41], we assume that the magnetization pattern of the nanodisk consists of a meronlike configuration, which can be well described by the following ansatz [48]:

$$\Theta(\rho) = \arccos\left(\frac{p}{1 + \left(\frac{\rho}{r_0}\right)^s}\right),$$

$$\Phi(\phi) = (q - 1)\phi + \gamma, \qquad (4)$$

where q is the winding number of the magnetic configuration, and represents the curl of the field around the meron's core when projecting the field onto the surface. Therefore, a vortex or antivortex structure can be described for $q = 1$ or $q = -1$, respectively (see Fig. 1). The meron is also characterized by the polarity p of the core, which can be 1 or -1 when the central magnetic moment points parallel or antiparallel to $\mathbf{n}$. It can be noticed that the magnetization field is parametrized in terms of a curvilinear basis. Therefore, the parabolic/hyperbolic deformation of the elastic subsystem produces a similar symmetry of deformation for the magnetic subsystem. Similar magnetization parametrizations of vortices have been used to describe vortices in paraboloidal [49] and spherical [50] magnetic nanoparticles. The chirality of the meron is determined by the parameter γ, which consists of a phase that gives the orientation of the field with respect to the radial direction $\vec{\rho}$ on the surface. The parameter s is a positive integer that determines the meron's core size, with radius r_0, and is defined as the minimum radial distance between the surface's center and that when $\mathbf{m} \cdot \vec{n} = 0$ occurs. The described magnetization vector field for different values of q and γ, hosted in structures with different curvatures is presented in Fig. 1. The meron's core is represented by the smaller yellow circle. The adopted ansatz describing the meron's profile defines a vortex (antivortex) as a configuration that lies asymptotically in the in-surface direction.

The total energy of the system is given by $E = E_m + E_{el}$, where E_m and E_{el} are respectively the magnetic and elastic contributions to the total energy. Since we are dealing with very thin shells, we can approximate the dipolar energy by an easy-surface anisotropy. Therefore, the magnetic contribution to the total energy is determined by the exchange and effective anisotropy, given respectively by

$$E_x = Ah \int g^{\mu\nu} \frac{\partial \mathbf{m}}{\partial x_\mu} \cdot \frac{\partial \mathbf{m}}{\partial x_\nu} \sqrt{g}\, dx_\mu\, dx_\nu \qquad (5)$$

and

$$E_{ani} = K_a h \int (\mathbf{m} \cdot \mathbf{n})^2 \sqrt{g}\, d\rho\, d\phi, \qquad (6)$$

where the Einstein summation convention over repeated indices is assumed. The parameter A is the exchange stiffness. Considering that for thin films the magnetostatic contribution can be reduced to an effective easy-surface anisotropy [51], we adopt $K_a = \mu_0 M_s^2 / 2$. Additionally, $\sqrt{g} = \sqrt{\|\det g_{\mu\nu}\|}$, and the covariant ($g_{\mu\nu}$) and contravariant ($g^{\mu\nu}$) metric elements are obtained from the parametrization given in Eq. (1) (see Appendix A for details on the calculation of these geometrical quantities). The competition between exchange and anisotropy interactions characterizes a magnetic length $\ell = \sqrt{A/K_a}$, which determines the length scale of the system (and the core's size of the meron configuration).

The elastic energy of flexible systems is determined from the sum of different terms regarding energy costs appearing in the system when it deforms. It is important to note that three-dimensional (3D) architectures as curved systems are fabricated using a strategic and consolidated route, which induces a strain gradient across the bilayers [52]. Such systems have a tensile and compressive hybrid state along the radial direction simultaneously without any need to maintain externally applied strain. This complex strain state is associated with the geometric configuration of these systems, such as rolled-up tubes [52], where the diameter can be dimensioned through the control of the built-in elastic strain distribution that arises due to lattice mismatch between bilayers and bilayer thickness [53,54]. However, in our work, we consider a quasi-2D system, and we do not take into account the complex strain distribution along the normal direction, as discussed in Sec. II. In this context, the magnetization is uniform along the normal direction, and the physical effects of this thin disk emerge from the system curvature. Under these assumptions, the elastic energy is determined from the approximation for 2D systems [32,55,56], given by the sum between stretching and bending energies, as follows:

$$E_{el} = \int [h\, w_s + h^3\, w_b] \sqrt{g}\, d\rho\, d\phi, \qquad (7)$$

where the stretching and bending energy densities are respectively

$$w_s = \frac{Y}{8(1+\varsigma)} \left(\frac{\varsigma}{1-\varsigma} \bar{g}^{\alpha\beta} \bar{g}^{\gamma\delta} + \bar{g}^{\alpha\gamma} \bar{g}^{\beta\delta} \right)$$
$$\times (g_{\alpha\beta} - \bar{g}_{\alpha\beta})(g_{\gamma\delta} - \bar{g}_{\gamma\delta}) \qquad (8)$$

and

$$w_b = \frac{Y\, b_{\alpha\beta} b_{\gamma\delta}}{24(1+\varsigma)} \left(\frac{\varsigma}{1-\varsigma} \bar{g}^{\alpha\beta} \bar{g}^{\gamma\delta} + \bar{g}^{\alpha\gamma} \bar{g}^{\beta\delta} \right). \qquad (9)$$

Here, the parameters Y and ς are Young's modulus and the Poisson ratio [57], respectively, and $b_{\mu\nu} = \mathbf{n} \cdot \partial_\mu \mathbf{g}_\nu$. In addition, $\bar{g}_{\mu\nu}$ is the metric tensor for a nanodisk without deformation. From Eqs. (8) and (9), one

can notice that both stretching and bending terms of the elastic energy increase with Young's modulus when the planar disk deforms to the paraboloid or hyperbolic paraboloid geometries. Additionally, because we focus on analyzing deformations of a very thin structure, the stretching energy (proportional to h) is much bigger than the bending cost (proportional to h^3) to deform the flexible magnetic disk. The explicit elastic energy density expressions written in terms of the geometrical parameters of the considered structures are cumbersome and therefore they are presented in Appendix A. An important point is that both magnetic and elastic subsystems interact through the anisotropy energy.

III. RESULTS

A. Winding-number-induced curvature

The model described above allows us to determine the magnetic and elastic properties of the considered structures by calculating the total energy as a function of different geometrical and material parameters. All results presented in this section were obtained through numerical calculations of the total energy of the flexible magnetic system and consider a Poisson ratio $\varsigma = 1/3$. For each value of c, we have evaluated the meron's core radius minimizing the energy. Several results presented in this work regard the optimum curvature c^*, defined as the value of c that minimizes the total energy for a given set of parameters. In the numerical calculations we have used the magnetic parameters of Permalloy [58], that is, $A = 10$ pJ/m and $M_s = 800$ kA/m. To analyze the influence of a range of parameters in the possibility of controlling the shape of a flexible magnetic membrane through modifying its magnetization configuration, we have considered different values for the Young's modulus. Depending on the nanodisk geometrical parameters, the magnetic vortex-like distribution can appear as the ground state in the magnetic disk, while the antivortex-like magnetization distribution can be the ground state in asteroid-like geometries [59,60]. Additionally, curved systems present effective chiral interactions that produce a curvature-induced selection on merons [41] in such a way that vortices are energetically more favorable on surfaces with positive Gaussian curvatures, while antivortices appear on surfaces with negative ones. Therefore, to present a complete analysis of magnetization profile influence on the system geometry, we analyze the total energy of both vortex and antivortex metastable states for the complete range of the considered values of c. Additionally, in all examined cases, the presented results regard the meron's core size that minimizes the magnetic energy, ensuring that we are considering a magnetic metastable state. Finally, the results presented in this section regard merons with $p = +1$ and $\gamma = 0$.

First, we determine the behavior of the total energy as a function of the disk radius R for a fixed value of $h = 0.1\ell$, and $A/(Yh^2) = 40$. The obtained results are depicted in Fig. 2 for $R = 4\ell$ (a), 6ℓ (b), 8ℓ (c), and 10ℓ (d). In all cases, we observe that the meron's winding number determines the curvature's sign that minimizes the total energy. That is, vortices make the flexible magnetic nanodisks assume a shape with positive Gaussian curvature, while the antivortex yields a disk deformation to surfaces with negative curvature. These
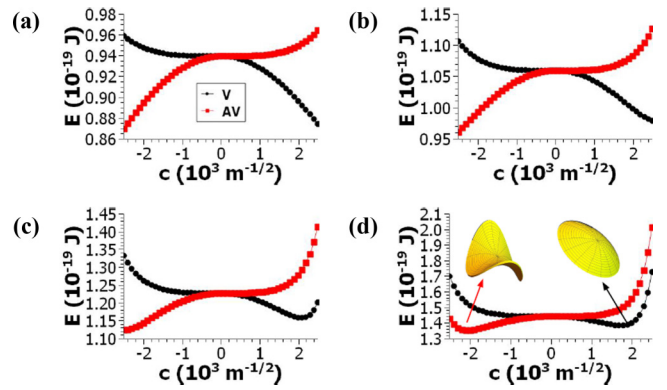

FIG. 2. Total energy as a function of c for different disk radius. Panels (a), (b), (c), and (d) present the results for $R = 4\ell$, 6ℓ, 8ℓ, and 10ℓ, respectively. The thickness is $h = 0.1\ell$, and $A/(Yh^2) = 40$.

results agree with those obtained by Elías *et al.* [41], which considered merons hosted in rigid structures, showing the emergence of a curvature-induced selection of the meron's winding number. In the present study, the radius dependence of the curvature minimizing the total energy results from the competition between magnetic and elastic interactions. While the magnetic energy diminishes as $|c|$ increases, the elastic energy cost to deform the nanostructure increases as a function of $|c|$. From the analysis of Figs. 2(a) and 2(b), the flexible magnetic structure deforms until its curvature reaches the maximum value in the considered range ($c = 2.5 \times 10^3$ m$^{-1/2}$). This behavior can be explained by the high energy cost to nucleate the meron's core, which, for small radii, occupies a substantial area in the nanodisk in comparison with its external radius. Therefore, the structure presents a large deformation to diminish the anisotropic energy. As the radius of the nanostructure increases, the meron's core energy gives a lower contribution compared to other energy terms. Therefore, there is a limit in the maximum curvature that the flexible magnetic disk can reach. For instance, Fig. 2(d) reveals that a nanodisk with an external radius of 10ℓ can deform until it reaches a curvature of $c \approx 1.8 \times 10^3$ m$^{-1/2}$ or $c \approx -2.1 \times 10^3$ m$^{-1/2}$ when it hosts a vortex or an antivortex, respectively. The insets in Fig. 2(d) show the surface shape for the minimum energy states. The obtained value of c for the minimum energy configuration is associated with a pronounced increase in the stretching energy near to this value (see Fig. 6 in Appendix B). Therefore, when the structure reaches the curvature determined by this value of c, the elastic term to the total energy dominates, defining the stable shape of the system.

Let us now explore the impact of changes on the mechanical properties in the deformation of the flexible magnetic membrane. Specifically, we are interested in studying the optimum curvature (c^*) dependence on the effect of changing Young's modulus, which is the parameter controlling the elastic stiffness of the material under external forces. In this context, in Fig. 3 we depict the total energy of the system as a function of the curvature for four distinct values of Y. As expected, for small Young's modulus [$A/(Yh^2) = 400$], the reached optimum curvature does not appear in the range of parameters considered here, evidencing that the nanostructure
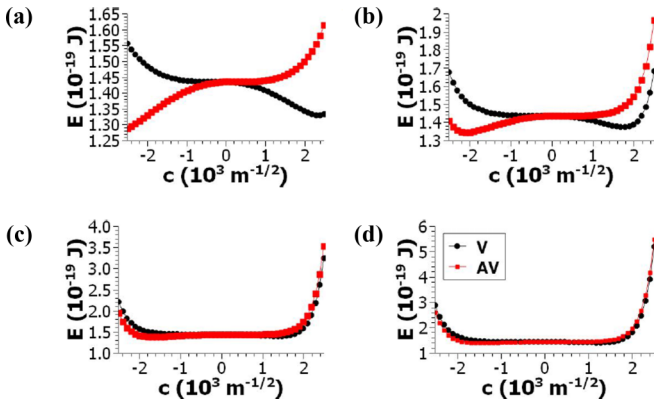
FIG. 3. System energy as a function of the curvature for a nanodisk with radius $R = 10\ell$ and $h = 0.1\ell$ for different Young's modulus. Panels (a), (b), (c), and (d) depict a nanostructure with $A/(Yh^2) = 400, 40, 8,$ and 4, respectively.
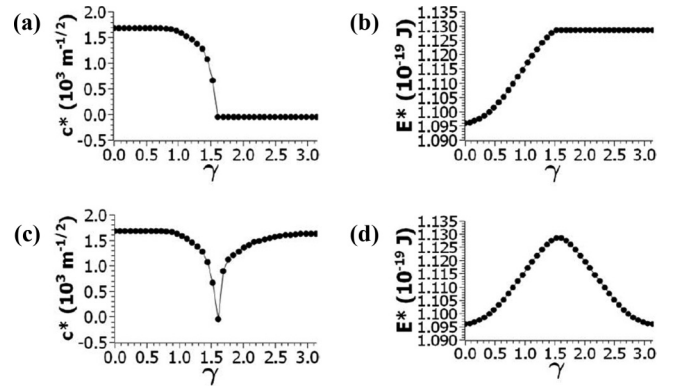

FIG. 4. Optimum curvature [(a) and (c)] and total energy [(b) and (d)] as a function of γ for an unchanged (top graphics) and variable (bottom graphics) polarity.

deforms until it reaches high values of $|c|$ [see Fig. 3(a)]. Figures 3(b) and 3(c) present the obtained results for $A/(Yh^2) = 40$ and $A/(Yh^2) = 8$, respectively. One can notice that the optimum curvature of the system decreases as the Young's modulus increases. That is, the curvature that minimizes the energy diminishes in modulus, indicating the increase in the structure rigidity. Indeed, the greater the value Y, the smaller the value of c for which the stretching energy presents a pronounced increase (see Appendix B for details). Finally, for $A/(Yh^2) = 4$ [Fig. 3(d)], the elastic energy cost to deform the nanostructure is very high, and the nanodisk shape becomes independent of the winding number of the hosted meron, which eventually reads the optimum curvature $|c^*| \approx 0$.

From the obtained results, one can see that depending on the meron's winding number, the flexible disk with $R = 10\ell$ and $A/(Yh^2) = 40$, hosting antivortices or vortices as metastable states, deforms until it reaches optimum curvatures in the range of $c^* \in [-2.1 \times 10^3, 1.8 \times 10^3]$ m$^{-1/2}$. This change in the system curvature yields a stretching in the nanodisk, evidenced by the increase in the area of the flexible system when it curves. We have then calculated the variation in the area of the structure, obtaining $\Delta A/A_0 = 100[A(c) - A_0]/A_0 \in [2\%, 6\%]$, where $A(c)$ is the area of the structure with curvature c^* and A_0 is the area of the planar nanodisk.

Because the magnetic texture can determine the shape of a flexible magnetic system, we have also analyzed the possibility of deformations in nanodisks made of Permalloy, whose magnetoelastic properties are similar to those of bulk Fe$_{83}$Ga$_{17}$ ($Y = 100$ GPa) [58]. Our results suggest that the influence of the magnetic subsystem on the elastic one yields a slight deformation in these nanodots. Indeed, we have obtained that when a vortex is nucleated in this structure, the optimum curvature of the system reveals a tiny deformation on the order of $\lesssim 10^{-11}$ m in the nanodot diameter.

B. Influence of chirality on curvature

A remarkable feature of curved magnetic shells is the appearance of exchange-driven effective anisotropy and Dzyaloshinskii-Moriya interactions [33], which are respon-

sible, for instance, for the increase in the skyrmion stability in hills and valleys [35,36], and the emergence of curvature-induced forces in particlelike magnetization configurations [61,62]. Additionally, such effective interactions yield a curvature-induced phase selection in the domain wall (DW) phase, where the kind of DW head-to-head or tail-to-tail are always directed outward and inward from the bend, respectively [37]. Moreover, this phase selectivity also determines a polarity-chirality connection, where depending on the vortex chirality, there is a preferential direction for where its core points [34,41].

Based on the above described, we explore the possibility of manipulating the shape of the flexible magnetic particle by using meronlike configurations with a fixed polarity $p = 1$ (outward) and controlling the vortex chirality. It is worth noticing that although the dipolar interaction related to magnetostatic charges appearing at the borders of the disk fixes the vortex chirality in two values ($\gamma = \pm\pi/2$), the dipolar cost to host vortices with different chiralities in very thin flexible magnetic systems is small. Therefore, external stimuli (i.e., external magnetic fields) could produce smooth changes in the vortex chirality depending on the competition between this small magnetostatic interaction and the extra energy coming from the external stimulus. To better understand the influence of the vortex chirality on the optimum curvature, before analyzing the shape of the nanostructure as a function of the vortex chirality in the presence of external stimuli, we have studied how the vortex chirality influences the shape of the nanostructure in the absence of a magnetic field. In Fig. 4 we have obtained both the optimum curvature c^* and the total energy when the system reaches its optimum curvature E^* as a function of γ for a nanodisk with $R = 10\ell$, $h = 0.1\ell$, and $A/(Yh)^2 = 40$. The analysis of Fig. 4(a) reveals that changes in the vortex chirality yield a variation in the shape of the nanostructure, including a change in the curvature sign when $\gamma = \pi/2$. Therefore, the flexible magnetic system changes its shape from a paraboloid-like to a saddle-like geometry. To understand this chirality-induced shape variation, we have determined the total energy as a function of γ, whose results are presented in Fig. 4(b), revealing that the energy increases with γ. Thus, when hosting a vortex state for certain values of γ, the system is deformed in a negatively curved surface to
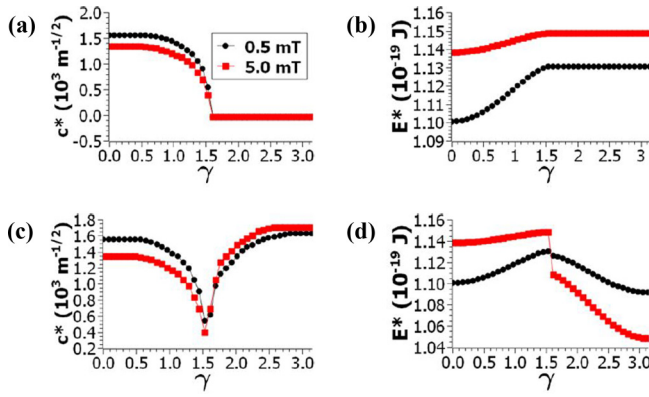
FIG. 5. Optimum curvature and total energy for fixed [(a) and (b)] and variable [(c) and (d)] polarity as a function of the vortex chirality for a nanodisk under the action of a magnetic field $\mathbf{B} = -B\hat{\mathbf{z}}$. Black dots and red squares represent the results for $B = 0.5$ mT and $B = 5.0$ mT, respectively.

control the increase in the magnetic energy due to the polarity-chirality connection [34,41]. To prove the above statement, we have analyzed the optimum curvature and the total energy as a function of γ, but now, we consider a change in the vortex polarity from $p = 1$ to $p = -1$ when $\gamma = \pi/2$. In this case, as presented in Figs. 4(c) and 4(d), we observe that this change in the vortex polarity makes the system remain with positive curvature for any value of γ.

An external magnetic field can drive the proper control of the vortex chirality and polarity [63–65]. Therefore, we have analyzed the effects that a uniform magnetic field applied along the z-axis direction produces on the shape of the nanodisk hosting a vortex as a magnetization state. In this context, we determine the optimum curvature as a function of the vortex chirality for a flexible magnetic nanodisk under the action of an external magnetic field $\mathbf{B} = -B\hat{\mathbf{z}}$. Figures 5(a) and 5(b) show, respectively, the optimum curvature and total energy as a function of the vortex chirality (γ) when we fix its polarity $p = +1$. Red squares and black dots show the behavior of a nanodisk under the action of a magnetic field of strength 0.5 mT (black dots) and 5 mT (red squares), respectively. It can be noticed that the obtained optimum curvature is a result of the competition between the curvature-induced polarity-chirality connection and Zeeman interaction. That is, a direct comparison between Figs. 4(a) and 5(a) evidences that the magnetic field forces the system to diminish the modulus of its optimum curvature for all values of γ. Additionally, because the magnetic field direction favors the magnetic moments pointing along the $-\mathbf{z}$ direction, the optimum curvature is positive for any value of γ, if we consider that the polarity changes when $\gamma \geqslant \pi/2$. In this case, c^* increases as function of the magnetic field [see Fig. 5(c)]. Finally, as expected, when the vortex polarity changes and points along the magnetic field direction, the total energy decreases, evidencing that this state minimizes both Zeeman and exchange interactions in the magnetic subsystem [see Fig. 5(d)].

From the above results, one can propose that such flexible magnetic systems could be used in applications such as small-scale robotics. Indeed, the actuation of the nanodisk could be performed, for instance, by applying an external magnetic

field controlling the vortex chirality (γ) and/or polarity (p). The chirality-polarity connection of a magnetic vortex could produce changes in the shape of the nanodisk from a structure with negative to a system presenting positive curvature, depending on the relative directions of the magnetization, determined by γ and p.

IV. CONCLUSIONS

We studied the properties of a flexible magnetic nanodisk hosting merons as a magnetic state for a large range of geometrical, elastic, and magnetic parameters. Although we did not analyze the stability of the meron's magnetic state in the considered system, we claim that such configurations can be, at least, artificially imposed and hosted in a nanodisk, as evidenced by the presence of metastable (stable) antivortices (vortices) in nanodisks [46,47,66]. Thus, interesting results regarding the interplay between magnetic and elastic subsystems were presented that should be considered even if the magnetic states have a finite lifetime. It is obtained that in the absence of an external magnetic field, the meron's winding number curvature determines whether the nanoparticle's shape presents a positive or negative curvature. Additionally, the optimum curvature adopted by the nanodisk is a function of its radius, Young's modulus, and the meron's chirality. It was obtained that due to an increase in the stretching energy as a function of the system curvature, the absolute value of the system's optimum curvature decreases with the Young's modulus. Therefore, because the Young's modulus value influences the deformation magnitudes, our model is sensitive to this parameter, and, within linear elasticity theory, more significant effects can be expected as Young's modulus is greater.

It was also shown that due to the exchange-driven curvature-induced effective DMI, changes in the vortex chirality yield changes in the nanoparticle's shape. Finally, it was shown that external magnetic fields can be used to change the nanoparticle's shape by the proper control of the vortex chirality. Indeed, because uniform magnetic fields favor the parallel magnetic moments' alignment, the lower energy state is obtained when the Zeeman energy is favored while respecting the polarity-chirality connection.

The above-described results do not consider the shape's dynamical evolution of the flexible magnetic disk under the action of a magnetic field, but present several static properties of flexible magnetic disks hosting merons as magnetization states. We also call attention to the fact that this work has the limitation of considering deformations of the magnetization textures using a specific basis to parametrize the geometry of flexible magnetic disks. Nevertheless, the main focus of our work is describing the main aspects of the interaction between elastic and magnetic subsystems in the surface curvature of circular thin structure hosting a meron magnetic texture. Thus, as a first approximation, we have successfully described how specific deformations emerge when changing the magnetic configuration. A complete study considering different coordinate systems to parametrize different deformations to the nanostructure and the magnetization texture would be interesting for future works.

APPENDIX A: GEOMETRICAL ASPECTS OF THE CONSIDERED STRUCTURES AND EXPRESSIONS FOR ENERGY DENSITIES

1. Metric elements

The considered structures are parametrized by Eq. (1), which allows us to obtain the covariant metric matrix, given by

$$g = \begin{pmatrix} g_{11} & g_{12} \\ g_{21} & g_{22} \end{pmatrix}, \tag{A1}$$

where

$$g_{11} = 1 + 4\rho^2 (c^2 \cos^2 \phi + c|c| \sin^2 \phi)^2,$$
$$g_{12} = 2\rho^3 (c^2 \cos^2 \phi + c|c| \sin^2 \phi)(2c|c| - 2c^2),$$
$$g_{21} = g_{12},$$
$$g_{22} = \rho^2 [1 + (2c|c| - 2c^2)^2 \rho^2 \cos^2 \phi \sin^2 \phi]. \tag{A2}$$

It can be noticed that the metric elements of the reference system ($\bar{g}$) are obtained from taking $c = 0$ (planar disk) in the above equation. Therefore, we obtain $\bar{g}_{\rho\rho} = 1$, $\bar{g}_{\phi\phi} = \rho^2$, and $\bar{g}_{\rho\phi} = \bar{g}_{\phi\rho} = 0$. The contravariant metric elements $g^{\mu\nu}$ can be obtained from the relation $g^{\mu\nu} g_{\mu\nu} = \delta^\mu_\nu$.

2. Elastic energy densities

a. Stretching energy

The stretching energy consists of the cost to produce changes in the size of the elastic subsystem. In the adopted theoretical model, the stretching energy density can be obtained from substituting the metric elements given in Eq. (A2) in Eq. (8). After some algebra, we obtain

$$w_s = \frac{Y}{8(1-\nu)^2} [4\rho^2 (c^2 \cos^2 \phi + c|c| \sin^2 \phi)]^2. \tag{A3}$$

b. Bending energy density

The introduction of bends in the elastic subsystem also yields an energetic cost, the so-called bending energy, whose energy density is given in Eq. (9), where the matrix elements $b_{\mu\nu}$ are evaluated as

$$b_{11} = \frac{\partial^2}{\partial \rho^2} (\vec{r} \cdot \vec{n}),$$

$$b_{12} = b_{21} = \frac{\partial}{\partial \phi} \frac{\partial}{\partial \rho} (\vec{r} \cdot \vec{n}),$$
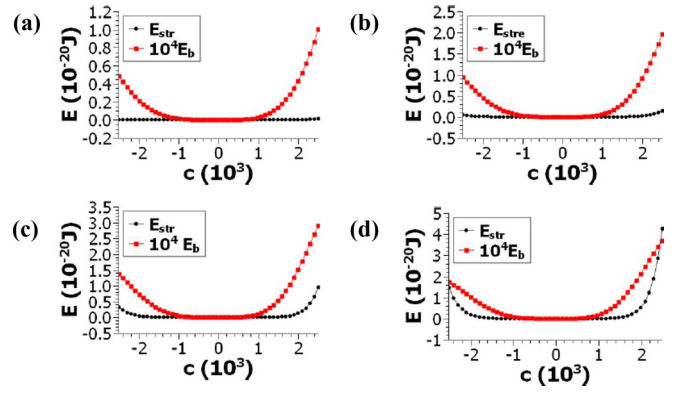

FIG. 6. Stretching E_{str} and bending energy E_b as a function of c for different disk radius. Panels (a), (b), (c), and (d) present the results for $R = 4\ell$, 6ℓ, 8ℓ, and 10ℓ, respectively. The thickness is $h = 0.1\ell$, and $A/(Yh^2) = 40$.

$$b_{22} = \frac{\partial^2}{\partial \phi^2} (\vec{r} \cdot \vec{n}). \tag{A4}$$

Therefore, the substitution of the metric elements and the matrix elements $b + \mu\nu$ in Eq. (9) leads to the bending energy density written as

$$w_b(\rho, \phi) = \frac{Y}{24(1+\nu)} \left[\frac{1}{1-\nu} b_{11}^2 + \rho^{-4} b_{22} b_{21} \right.$$
$$\left. + 2\frac{\nu}{1-\nu} \rho^{-2} b_{22} b_{11} + \rho^{-2} b_{12}^2 \right]. \tag{A5}$$

APPENDIX B: STRETCHING AND BENDING ENERGIES

The value of c for the minimum energy configuration presented in Fig. 2 can be understood from the separated analysis of the elastic term to the total energy. Therefore, we have obtained the stretching and bending energies as a function of c for $R = 4\ell$, 6ℓ, 8ℓ, and 10ℓ. The results are depicted in Fig. 6. Because the bending energy (E_b) is much smaller than the stretching term (E_s), in the obtained graphics we present the results for $10^4 E_b$ (red dots) and E_s (black squares).

Figures 6(a) and 6(b) evidence that for systems with small values of Y, the stretching energy almost does not present variations when the system deforms. Additionally, despite that the bending energy presents pronounced variations in the interval of values of c considered in this work, it is an order of magnitude smaller than the other terms to the energy, and therefore the minimum energy configuration is determined by the magnetic energy (see Fig. 2). On the other hand, as Y increases, one can observe a pronounced increase in the stretching energy [see Figs. 6(c) and 6(d)]. In this case, the competition between magnetic and elastic subsystems determines the value of c that minimizes the total energy and the final shape of the nanostructure.

[1] D. Makarov, M. Melzer, D. Karnaushenko, and O. G. Schmidt, Shapeable magnetoelectronics, Appl. Phys. Rev. **3**, 011101 (2016).

[2] P. Bujak, I. Kulszewicz-Bajer, M. Zagorska, V. Maurel, I. Wielgus, and A. Pron, Polymers for electronics and spintronics, Chem. Soc. Rev. **42**, 8895 (2013).

[3] M. Melzer, M. Kaltenbrunner, D. Makarov, D. Karnaushenko, D. Karnaushenko, T. Sekitani, T. Someya, and O. G. Schmidt, Imperceptible magnetoelectronics, Nat. Commun. **6**, 6080 (2015).

[4] H. Vandeparre, D. Watson, and S. P. Lacoura, Extremely robust and conformable capacitive pressure sensors based on flexible polyurethane foams and stretchable metallization, Appl. Phys. Lett. **103**, 204103 (2013).

[5] R. C. Webb, A. P. Bonifas, A. Behnaz, Y. Zhang, K. J. Yu, H. Cheng, M. Shi, Z. Bian, Z. Liu, Y.-S. Kim, W.-H. Yeo, J. S. Park, J. Song, Y. Li, Y. Huang, A. M. Gorbach, and J. A. Rogers, Ultrathin conformal devices for precise and continuous thermal characterization of human skin, Nat. Mater. **12**, 938 (2013).

[6] O. Graudejus, Z. Yu, J. Jones, B. Morrison, and S. Wagner, Characterization of an elastically stretchable microelectrode array and its application to neural field potential recordings, J. Electrochem. Soc. **156**, P85 (2009).

[7] D. J. Lipomi, M. Vosgueritchian, B. C-K. Tee, S. L. Hellstrom, J. A. Lee, C. H. Fox, and Z. Bao, Skin-like pressure and strain sensors based on transparent elastic films of carbon nanotubes, Nat. Nanotechnol. **6**, 788 (2011).

[8] V. J. Lumelsky, M. S. Shur, and S. Wagner, Sensitive skin, IEEE Sens. J. **1**, 41 (2001).

[9] M. L. Hammock, A. Chortos, B. C. K. Tee, J. B. H. Tok, and Z. A. Bao, The evolution of electronic skin (e-skin): A brief history, design considerations, and recent progress, Adv. Mater. **25**, 5997 (2013).

[10] M.-G. Kim, H. Alrowais, and O. Brand, 3D-integrated and multifunctional all-soft physical microsystems based on liquid metal for electronic skin applications, Adv. Electron. Mater. **4**, 1700434 (2018).

[11] W. Hu, G. Z. Lum, M. Mastrangeli, and M. Sitti, Small-scale soft-bodied robot with multimodal locomotion, Nature (London) **554**, 81 (2018).

[12] S. Gong, W. Schwalb, Y. W. Wang, Y. Chen, Y. Tang, J. Si, B. Shirinzadeh, and W. L. Cheng, A wearable and highly sensitive pressure sensor with ultrathin gold nanowires, Nat. Commun. **5**, 3132 (2014).

[13] Y. Timounay, A. R. Hartwell, M. He, D. E. King, L. K. Murphy, V. Démery, and J. D. Paulsen, Sculpting Liquids with Ultrathin Shells, Phys. Rev. Lett. **127**, 108002 (2021).

[14] S. Schuhladen, F. Preller, R. Rix, S. Petsch, R. Zentel, and H. Zappe, Adv. Mater. **26**, 7247 (2014).

[15] G. Z. Lum, Z. Ye, X. Dong, H. Marvi, O. Erin, W. Hu, and M. Sitti, Proc. Natl. Acad. Sci. USA **113**, E6007 (2016).

[16] R. Geryak and V. V. Tsukruk, Reconfigurable and actuating structures from soft materials, Soft Matter **10**, 1246 (2014).

[17] D. Romeis, P. Metsch, M. Kästner, and M. Saphiannikova, Theoretical models for magneto-sensitive elastomers: A comparison between continuum and dipole approaches, Phys. Rev. E **95**, 042501 (2017).

[18] E. Coquelle and G. Bossis, Magnetostriction and piezoresistivity in elastomers filled with magnetic particles, J. Adv. Sci. **17**, 132 (2005).

[19] S. Chougale, D. Romeis, and M. Saphiannikova, Transverse isotropy in magnetoactive elastomers, J. Magn. Magn. Mater. **523**, 167597 (2021).

[20] C. A. Brisbois, M. Tasinkevych, P. Vázquez-Montejo, and M. O. de la Cruz, Actuation of magnetoelastic membranes in precessing magnetic fields, Proc. Natl. Acad. Sci. USA **116**, 2500 (2019).

[21] R. Podgajny, M. Bałanda, M. Sikora, M. Borowiec, L. Spałek, C. Kapusta, and B. Sieklucka, Cobalt(II) octacyanotungstate(V) organic-inorganic hybrid ferromagnetic materials with pyrazine and 4,4'-bipyridine, Dalton Trans. **23**, 2801 (2006).

[22] L. D. Barron, Chirality and magnetism shake hands, Nat. Mater. **7**, 691 (2008).

[23] J. S. Miller, Magnetically ordered molecule-based materials, Chem. Soc. Rev. **40**, 3266 (2011).

[24] J. S. Miller, Organic- and molecule-based magnets, Mater. Today **17**, 224 (2014).

[25] J. Mahmood, J. Park, D. Shin, H.-J. Choi, J.-M. Seo, J.-W. Yoo, and J.-B. Baek, Organic ferromagnetism: Trapping spins in the glassy state of an organic network structure, Chem **4**, 2357 (2018).

[26] R. Dandoloff, S. Villain-Guillot, A. Saxena, and A. R. Bishop, Violation of Self-Duality for Topological Solitons Due to Soliton-Soliton Interaction on a Cylindrical Geometry, Phys. Rev. Lett. **74**, 813 (1995).

[27] A. Saxena and R. Dandoloff, Curvature-induced geometrical frustration in magnetic systems, Phys. Rev. B **55**, 11049 (1997).

[28] A. Saxena, R. Dandoloff, and T. Lookman, Deformable curved magnetic surfaces, Physica A **261**, 13 (1998).

[29] V. L. Carvalho-Santos and R. Dandoloff, Topological spin excitations induced by an external magnetic field coupled to a surface with rotational symmetry, Braz. J. Phys. **43**, 130 (2013).

[30] P. S. C. Vilas-Boas, R. G. Elias, D. Altbir, J. M. Fonseca, and V. L. Carvalho-Santos, Topological magnetic solitons on a paraboloidal shell, Phys. Lett. A **379**, 47 (2015).

[31] Y. Gaididei, K. V. Yershov, D. D. Sheka, V. P. Kravchuk, and A. Saxena, Magnetization-induced shape transformations in flexible ferromagnetic rings, Phys. Rev. B **99**, 014404 (2019).

[32] K. V. Yershov, V. P. Kravchuk, D. D. Sheka, J. van den Brink, and Y. Gaididei, Spontaneous deformation of flexible ferromagnetic ribbons induced by Dzyaloshinskii-Moriya interaction, Phys. Rev. B **100**, 140407(R) (2019).

[33] Y. Gaididei, V. P. Kravchuk, and D. D. Sheka, Curvature Effects in Thin Magnetic Shells, Phys. Rev. Lett. **112**, 257203 (2014).

[34] M. I. Sloika, V. P. Kravchuk, D. D. Sheka, and Y. Gaididei, Curvature induced chirality symmetry breaking in vortex core switching phenomena, Appl. Phys. Lett. **104**, 252403 (2014).

[35] V. L. Carvalho-Santos, R. M. Corona, D. Altbir, and S. Castillo-Sepúlveda, Shifts in the skyrmion stabilization due to curvature effects in dome- and antidome-shaped surfaces, Phys. Rev. B **102**, 024444 (2020).

[36] V. P. Kravchuk, D. D. Sheka, A. Kákay, O. M. Volkov, U. K. Rößler, J. van den Brink, D. Makarov, and Y. Gaididei, Multiplet of Skyrmion States on a Curvilinear Defect: Reconfigurable Skyrmion Lattices, Phys. Rev. Lett. **120**, 067201 (2018).

[37] K. V. Yershov, V. P. Kravchuk, D. D. Sheka, and Y. Gaididei, Curvature-induced domain wall pinning, Phys. Rev. B **92**, 104412 (2015).

[38] R. Cacilhas, C. I. L. de Araujo, V. L. Carvalho-Santos, R. Moreno, O. Chubykalo-Fesenko, and D. Altbir, Controlling

domain wall oscillations in bent cylindrical magnetic wires, Phys. Rev. B **101**, 184418 (2020).

[39] G. H. R. Bittencourt, R. Moreno, R. Cacilhas, S. Castillo-Sepúlveda, O. Chubykalo-Fesenko, D. Altbir, and V. L. Carvalho-Santos, Curvature-induced emergence of a second critical field for domain wall dynamics in bent nanostripes, Appl. Phys. Lett. **118**, 142405 (2021).

[40] S. Vojkovic, V. L. Carvalho-Santos, J. M. Fonseca, and A. S. Nunez, J. Appl. Phys. **121**, 113906 (2017).

[41] R. G. Elías, N. Vidal-Silva, and V. L. Carvalho-Santos, Winding number selection on merons by Gaussian curvatures sign, Sci. Rep. **9**, 14309 (2019).

[42] G. Goia, and R. J. James, Micromagnetics of very thin films, Proc. R. Soc. London A **453**, 213 (1997).

[43] N. D. Mermin, The topological theory of defects in ordered media, Rev. Mod. Phys. **51**, 591 (1979).

[44] G. S. Milagre and W. A. Moura-Melo, Magnetic vortex-like excitations on a sphere, Phys. Lett. A **368**, 155 (2007).

[45] L. R. A. Belo, N. M. Oliveira-Neto, W. A. Moura-Melo, A. R. Pereira, and E. Ercolessi, Heisenberg model on a space with negative curvature: Topological spin textures on the pseudo-sphere, Phys. Lett. A **365**, 463 (2007).

[46] M. Pues and G. Meier, Magnetic antivortices, in *Atomic- and Nanoscale Magnetism* (Springer, Cham, 2018), pp. 299-323.

[47] A. Lyberatos, S. Komineas, and N. Papanicolaou, Precessing vortices and antivortices in ferromagnetic elements, J. Appl. Phys. **109**, 023911 (2011).

[48] P. Landeros, J. Escrig, D. Altbir, D. Laroze, J. d'Albuquerque e Castro, and P. Vargas, Scaling relations for magnetic nanoparticles, Phys. Rev. B **71**, 094435 (2005).

[49] V. L. Carvalho-Santos, R. G. Elías, J. M. Fonseca, and D. Altbir, Curvature-induced changes in the magnetic energy of vortices and skyrmions in paraboloidal nanoparticles, J. Appl. Phys. **117**, 17E518 (2015).

[50] V. P. Kravchuk, D. D. Sheka, R. Streubel, D. Makarov, O. G. Schmidt, and Y. Gaididei, Out-of-surface vortices in spherical shells, Phys. Rev. B **85**, 144433 (2012).

[51] K. V. Yershov, V. P. Kravchuk, D. D. Sheka, and U. K. Rößler, Curvature effects on phase transitions in chiral magnets, SciPost Phys. **9**, 043 (2020).

[52] L. N. Rodrigues, D. Scolfaro, L. da Conceição, A. Malachias, O. D. D. Couto, Jr., F. Iikawa, and C. Deneke, Rolled up quantum wells composed of nanolayered InGaAs/GaAs heterostructures as optical materials for quantum information technology, ACS Appl. Nano Mater. **4**, 3140 (2021).

[53] A. Malachias, C. Deneke, B. Krause, C. Mocuta, S. Kiravittaya, T. H. Metzger, and O. G. Schmidt, Direct strain and elastic energy evaluation in rolled-up semiconductor tubes by x-ray microdiffraction, Phys. Rev. B **79**, 035301 (2009).

[54] P. Cendula, S. Kiravittaya, I. Mönch, J. Schumann, and O. G. Schmidt, Directional roll-up of nanomembranes mediated by wrinkling, Nano Lett. **11**, 236 (2011).

[55] E. Efrati, E. Sharon, and R. Kupferman, Elastic theory of unconstrained non-Euclidean plates, J. Mech. Phys. Solids **57**, 762 (2009).

[56] S. Armon, E. Efrati, R. Kupferman, and E. Sharon, Geometry and mechanics in the opening of chiral seed pods, Science **333**, 1726 (2011).

[57] M. Doi, *Soft Matter Physics*, 1st ed. (Oxford University Press, Oxford, 2013).

[58] M. T. Bryan, J. Dean, and D. A. Allwood, Dynamics of stress-induced domain wall motion, Phys. Rev. B **85**, 144411 (2012).

[59] S. Gliga, M. Yan, R. Hertel, and C. M. Schneider, Ultrafast dynamics of a magnetic antivortex: Micromagnetic simulations, Phys. Rev. B **77**, 060404(R) (2008).

[60] K. Shigeto, T. Okuno, K. Mibu, T. Shinjo, and T. Ono, Magnetic force microscopy observation of antivortex core with perpendicular magnetization in patterned thin film of permalloy, Appl. Phys. Lett. **80**, 4190 (2002).

[61] V. L. Carvalho-Santos, M. A. Castro, D. Salazar-Aravena, D. Laroze, R. M. Corona, S. Allende, and D. Altbir, Skyrmion propagation along curved racetracks, Appl. Phys. Lett. **118**, 172407 (2021).

[62] K. V. Yershov, V. P. Kravchuk, D. D. Sheka, O. V. Pylypovskyi, D. Makarov, and Y. Gaididei, Geometry-induced motion of magnetic domain walls in curved nanostripes, Phys. Rev. B **98**, 060409(R) (2018).

[63] M. Jaafar, R. Yanes, D. Perez de Lara, O. Chubykalo-Fesenko, A. Asenjo, E. M. Gonzalez, J. V. Anguita, M. Vazquez, and J. L. Vicent, Control of the chirality and polarity of magnetic vortices in triangular nanodots Phys. Rev. B **81**, 054439 (2010).

[64] S. Agramunt-Puig, N. Del-Valle, C. Navau, and A. Sanchez, Controlling vortex chirality and polarity by geometry in magnetic nanodots, Appl. Phys. Lett. **104**, 012407 (2014).

[65] J. Li, Y. Wang, Z. Zhao, J. Cao, F. Zhu, and R. Tai, Independent control of the chirality and polarity for the magnetic vortex in symmetric nanodot pairs, IEEE Trans. Magn. **56**, 4300306 (2020).

[66] G. A. Riley, H. J. Jason Liu, M. A. Asmat-Uceda, A. Haldar, and K. S. Buchanan, Observation of the dynamic modes of a magnetic antivortex using Brillouin light scattering, Phys. Rev. B **92**, 064423 (2015).